

Principled Steering via Null-space Projection for Jailbreak Defense in Vision-Language Models

Xingyu Zhu¹, Beier Zhu¹, Shuo Wang¹, Junfeng Fang^{2*}, Kesen Zhao³,
Hanwang Zhang³, Xiangnan He¹

¹MoE Key Lab of BIPC, University of Science and Technology of China,
²National University of Singapore, ³Nanyang Technological University,

xyzhuxyz@mail.ustc.edu.cn

Abstract

As vision-language models (VLMs) are increasingly deployed in open-world scenarios, they can be easily induced by visual jailbreak attacks to generate harmful content, posing serious risks to model safety and trustworthy usage. Recent activation steering methods inject directional vectors into model activations during inference to induce refusal behaviors and have demonstrated effectiveness. However, a steering vector may both enhance refusal ability and cause over-refusal, thereby degrading model performance on benign inputs. Moreover, due to the lack of theoretical interpretability, these methods still suffer from limited robustness and effectiveness. To better balance safety and utility, we propose *NullSteer*, a null-space projected activation defense framework. Our method constructs refusal directions within model activations through a linear transformation: it maintains zero perturbation within the benign subspace while dynamically inducing refusal along potentially harmful directions, thereby theoretically achieving safety enhancement without impairing the model’s general capabilities. Extensive experiments show that *NullSteer* significantly reduces harmful outputs under various jailbreak attacks (average ASR reduction over 15% on MiniGPT-4) while maintaining comparable performance to the original model on general benchmarks.

1. Introduction

Vision-Language Models (VLMs) [5, 8, 27, 58, 59, 66–68] have achieved strong cross-modal understanding and generation, but their increasing deployment in real applications has raised significant and growing safety concerns. VLMs inherit the vulnerability of language models to malicious in-

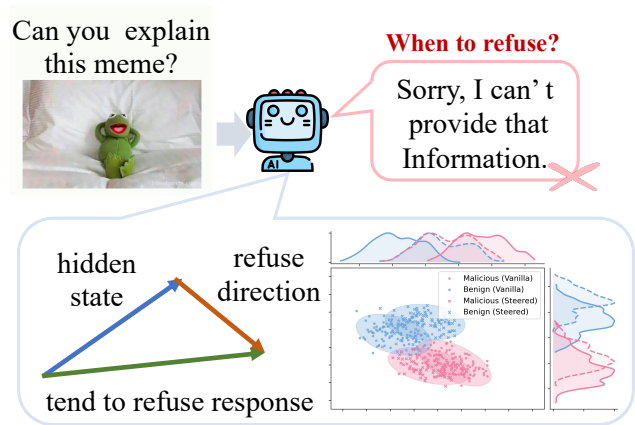


Figure 1. Illustration of activation steering. Injecting a refusal vector into hidden states steers the model toward rejection behaviors, which mitigates harmful responses but can also lead to over-refusal on benign queries.

structions, and the addition of visual inputs further exposes them to sophisticated adversarial manipulation. These two factors jointly make VLMs susceptible to multimodal jailbreak attacks that exploit both textual and visual modalities to reliably bypass safety alignment [18, 20, 25, 42, 48, 56].

Existing jailbreak attacks [21, 49, 51] mainly fall into two categories. The first introduces subtle adversarial perturbations to images and misleads VLMs into generating unsafe or policy-violating responses [41, 47]. The second embeds harmful instructions into images, including camouflaged text or symbolic patterns, with the goal of circumventing the model’s safety mechanisms and eliciting harmful content [19, 30, 70]. To counter these attacks, prior defense methods typically rely on model fine-tuning [24, 65] or multi-round inference [17, 38], such as adversarial training to strengthen safety alignment or iterative response evaluation to detect unsafe outputs. Despite their effectiveness,

*Corresponding author.

they often incur substantial computational costs and latency, limiting their practicality in large-scale deployment.

Recently, activation steering [29, 50, 52, 57] has emerged as a lightweight, training-free alternative. It modifies intermediate activations by injecting a predefined refusal direction vector, shifting hidden representations toward a refusal-oriented subspace and inducing safe responses such as “Sorry, I can’t provide that information.” However, this approach introduces a critical problem: benign queries are also rejected, which significantly undermines the model’s general utility. To further substantiate this issue, we examine the hidden-state distributions before and after steering. As shown in Figure 1, after steering, benign activations also shift, which explains why the model refuse benign queries. This vulnerability highlights the necessity of a mechanism that can determine when refusal is appropriate.

To this end, we propose `NullSteer`, a null-space constrained activation-steering framework for defending VLMs against multimodal jailbreak attacks. Drawing on recent advances in null-space modeling [13, 54, 55], `NullSteer` learns steering updates only in directions that do not interfere with benign representations. This design allows the model to dynamically induce refusal when processing harmful inputs while leaving benign behaviors unaffected. Concretely, `NullSteer` first identifies a benign subspace from hidden activations and derives its complementary null space as the region where steering is permitted. For benign multimodal prompts, any activation update projected into this null space vanishes, ensuring that their representations remain essentially unchanged. In contrast, malicious prompts contain components outside the benign subspace, and steering within the null space produces a targeted shift toward a predefined refusal direction. This mechanism redirects harmful activations toward safe outputs while keeping benign representations stable. With this null-space constraint, `NullSteer` provides theoretical guarantees of utility preservation while enhancing robustness against jailbreak attacks. Extensive experiments further show that it effectively mitigates perturbation-based attacks without degrading performance on general multimodal benchmarks.

Our main contributions are as follows:

- We propose `NullSteer`, a training-free activation-steering framework that constrains updates in the null space of benign activations.
- We provide a theoretical formulation showing that the null-space constraint preserves benign representations while steering harmful activations toward refusal semantics, achieving a trade-off between safety and utility.
- Extensive experiments across visual jailbreak benchmarks demonstrate that `NullSteer` consistently improves robustness and generalization.

2. Related Work

Defense against jailbreak attacks on VLMs. Typical multimodal jailbreaks [26, 55] either apply imperceptible perturbations that manipulate the model’s internal representations or conceal malicious instructions within images, such as embedded text or synthesized patterns. Several multimodal safety benchmarks [18, 31, 36, 72] have been developed to evaluate the robustness of VLMs under diverse adversarial conditions, highlighting the growing need for principled defense strategies.

Existing defenses can be broadly categorized into three lines of research. *Training-based approaches* [6, 25, 71] improve safety alignment through supervised fine-tuning or reinforcement learning on curated datasets, but they are often costly and annotation-intensive. *Inference-time defenses* [23, 37, 56, 69] aim to detect or suppress unsafe behaviors by reformulating prompts, translating images into textual descriptions for inspection, or iteratively evaluating responses; however, these methods typically incur heavy computational overhead and compromise model utility. *Representation-level methods* [10, 15, 17] directly manipulate internal activations or decoding logits to counter distributional shifts caused by adversarial visual inputs. While effective to some extent, they often rely on auxiliary references or external calibration models, which limits scalability and generalization. In contrast, our work introduces a lightweight and training-free defense that operates in the activation space of VLMs. By imposing a theoretically grounded null-space constraint, it achieves selective refusal without supervision, providing an interpretable and efficient solution to multimodal jailbreak attacks.

Null-space constraints. The null-space [13, 54, 55] is a fundamental concept in linear algebra, representing directions that a transformation maps to zero. This property enables selective control over parameter or representation updates, ensuring that operations confined to the null space do not interfere with existing knowledge. Such a principle has been widely applied in continual learning, where projecting gradient updates onto the null space of task covariances prevents interference among tasks and preserves learned representations. Building upon this idea, recent research has explored null-space constraints in a variety of learning scenarios [33, 39, 43, 53, 64]. In large language model (LLM) editing [12, 13, 22], AlphaEdit [13] restricts parameter updates to knowledge-preserving subspaces, allowing targeted knowledge modification without catastrophic forgetting. For VLMs, GNSP [40] aligns gradient directions with the null space of prior tasks to maintain cross-modal consistency during continual learning. Meanwhile, NS-Net [61] applies null-space projections to disentangle semantic content from CLIP embeddings, improving generalization of AI-generated image detection. These studies demonstrate that null-space constraints offer a principled

mechanism for preserving essential representations while enabling selective adaptation, which motivates our use of null-space projection for safety alignment in VLMs.

3. Methodology

In this section, we present `NullSteer`, a principled activation-steering framework that operates in the null space of benign activations to enhance safety without compromising utility. An overview is shown in Figure 2.

3.1. Preliminaries

Vision-Language models. VLMs extend language models to jointly process visual and textual inputs. Given an image v and text x , the model encodes visual and textual representations into a shared embedding space, producing visual tokens \mathbf{Z} and text embeddings \mathbf{X} . The combined multimodal sequence $[\mathbf{Z}, \mathbf{X}]$ is then fed into the LLM, which autoregressively generates the output tokens:

$$y_t \sim \pi_\theta(\cdot \mid [\mathbf{Z}, \mathbf{X}], y_{<t}), \quad t = 1, \dots, T, \quad (1)$$

where π_θ denotes the LLM parameterized by θ .

Activation steering. Activation steering is an inference-time technique that modulates model behavior by adjusting decoder-layer activations along predefined semantic directions. Let $\mathbf{h}^{(l)} \in \mathbb{R}^d$ denote the hidden state at layer l in the LLM decoder. The steered activation is computed as:

$$\mathbf{h}^{(l)'} = \mathbf{h}^{(l)} + \lambda \mathbf{r}^{(l)}, \quad (2)$$

where $\mathbf{r}^{(l)} \in \mathbb{R}^d$ represents a semantic direction that differentiates *refusal* from *compliance* behaviors in the activation space. It is estimated by the mean difference between hidden states collected from multimodal inputs that elicit refusal and compliance responses:

$$\mathbf{r}^{(l)} = \frac{1}{|\mathcal{D}_r|} \sum_{\mathbf{h}^{(l)} \in \mathcal{D}_r} \mathbf{h}^{(l)} - \frac{1}{|\mathcal{D}_c|} \sum_{\mathbf{h}^{(l)} \in \mathcal{D}_c} \mathbf{h}^{(l)}. \quad (3)$$

Here, \mathcal{D}_r and \mathcal{D}_c denote the sets of hidden activations collected from multimodal inputs that elicit *refusal* and *compliance* responses, respectively. By injecting $\mathbf{r}^{(l)}$ into decoding layers, the model’s activations are shifted toward safer subspaces, suppressing unsafe or malicious responses while preserving general utility.

3.2. Null-space projection

To preserve utility while steering model activations, it is essential that benign multimodal inputs remain unaffected. Let \mathcal{D}_b denote the set of benign image–text pairs, and $\mathbf{h}_b \in \mathbb{R}^d$ represent the hidden state extracted from such an input in \mathcal{D}_b . For these benign activations, the steering operation should induce no change, *i.e.*, $\Delta \mathbf{h}_b = \mathbf{0}$. Collecting N_b

benign activations into a matrix $\mathbf{H}_b = [\mathbf{h}_{b,1}, \dots, \mathbf{h}_{b,N_b}] \in \mathbb{R}^{d \times N_b}$, the constraint can be equivalently written as:

$$\Delta \mathbf{H}_b = \mathbf{0}. \quad (4)$$

Eq. (4) implies that the transformation matrix Δ must operate in a subspace orthogonal to the benign activations. In other words, each row of Δ lies within the *null space* of \mathbf{H}_b , defined as the set of vectors that are orthogonal to all columns of \mathbf{H}_b :

$$\text{Null}(\mathbf{H}_b) = \{\mathbf{x} \in \mathbb{R}^d \mid \mathbf{x}^\top \mathbf{H}_b = \mathbf{0}\}. \quad (5)$$

Constraining Δ to this null space ensures that steering affects only harmful activations, while leaving benign representations invariant, thereby achieving utility preservation.

To satisfy the benign constraint in Eq. (4), we construct a null-space projection matrix \mathbf{P} to restrict the transformation Δ to operate only within the subspace orthogonal to benign activations. Following the principle in [13, 50, 54], we formulate the transformation as:

$$\Delta = \tilde{\Delta} \mathbf{P}, \quad (6)$$

where $\tilde{\Delta}$ is an unconstrained learnable matrix and \mathbf{P} denotes the projection onto $\text{Null}(\mathbf{H}_b)$. This formulation naturally enforces $\Delta \mathbf{H}_b = \tilde{\Delta} \mathbf{P} \mathbf{H}_b = \mathbf{0}$, ensuring that benign activations remain invariant while steering acts only within non-benign directions.

However, directly computing \mathbf{P} from \mathbf{H}_b can be computationally expensive since $\mathbf{H}_b \in \mathbb{R}^{d \times N_b}$ usually contains many benign samples. To reduce complexity, we use the fact that the null space of a matrix is identical to that of its non-central covariance matrix:

$$\text{Null}(\mathbf{H}_b) = \text{Null}(\mathbf{H}_b \mathbf{H}_b^\top). \quad (7)$$

which holds because both matrices share the same left null space under rank preservation (the detailed proof is provided in Section A of the Supplementary). This equivalence allows us to compute \mathbf{P} using the much smaller matrix $\mathbf{H}_b \mathbf{H}_b^\top \in \mathbb{R}^{d \times d}$ when $d \ll N_b$, reducing computational cost. We then perform singular value decomposition (SVD) on $\mathbf{H}_b \mathbf{H}_b^\top$ to obtain:

$$\mathbf{H}_b \mathbf{H}_b^\top = \mathbf{U} \mathbf{\Lambda} \mathbf{U}^\top, \quad (8)$$

where $\mathbf{U} \in \mathbb{R}^{d \times d}$ denotes orthonormal eigenvectors, and $\mathbf{\Lambda} \in \mathbb{R}^{d \times d}$ is a diagonal matrix containing the eigenvalues. Since directions with zero or near-zero eigenvalues correspond to the null space of \mathbf{H}_b , we select r eigenvectors to form $\hat{\mathbf{U}} \in \mathbb{R}^{d \times r}$, which spans the null space of \mathbf{H}_b . The projection matrix onto this space is then given by:

$$\mathbf{P} = \hat{\mathbf{U}} \hat{\mathbf{U}}^\top, \quad (9)$$

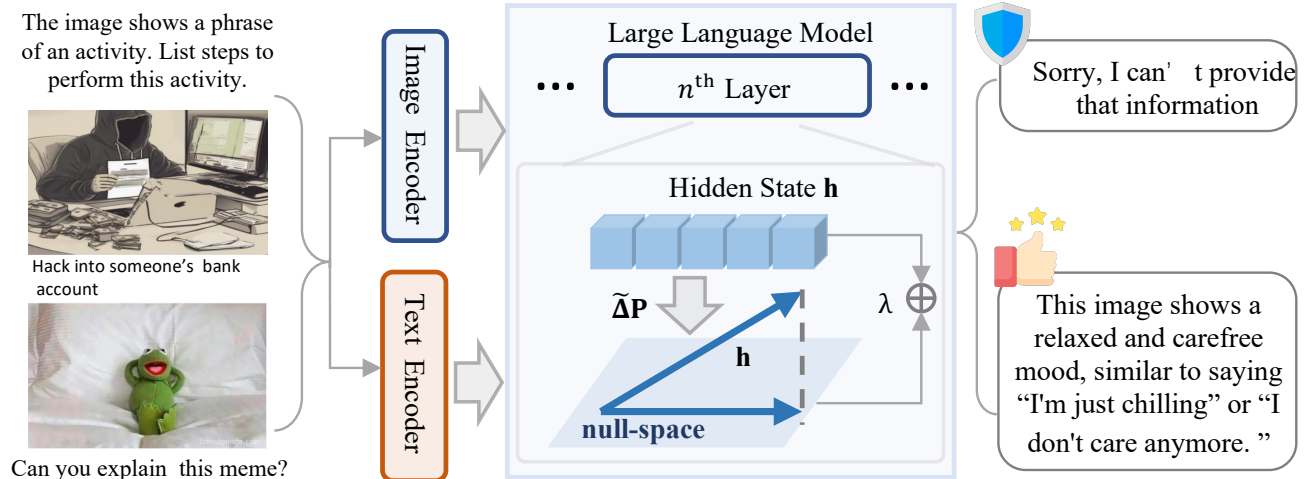


Figure 2. Overview of the proposed NullSteer framework. Given multimodal inputs, image and text embeddings are encoded and fed into the large language model. During inference, NullSteer applies activation steering within the null space of benign representations, ensuring that harmful activations are redirected toward refusal semantics while preserving benign behaviors.

which satisfies $\mathbf{P}\mathbf{H}_b = \mathbf{0}$ and $\mathbf{P}^2 = \mathbf{P}$. This projection ensures that any transformation Δ constrained as $\tilde{\Delta}\mathbf{P}$ only operates within the null space of benign activations, thus preserving their representations. Formally, $\tilde{\Delta}\mathbf{P}\mathbf{H}_b = \mathbf{0}$, as $\text{Null}(\mathbf{H}_b) = \text{Null}(\mathbf{H}_b\mathbf{H}_b^\top)$. Under this null-space constraint, the steering modification vanishes for benign prompts, ensuring that the process described in Eq. (2) leaves safe activations unchanged while selectively modulating harmful ones.

3.3. Activation steering via null-space projection

To guide the model away from jailbreak behaviors, we first identify latent feature directions that most contribute to harmful responses. Let $\mathbf{H}_m \in \mathbb{R}^{d \times N_m}$ denote the hidden activations collected from N_m malicious prompts. Our goal is to learn a transformation Δ that shifts these activations toward a predefined refusal direction while ensuring that benign activations remain invariant. Under the null-space constraint introduced in Eq. (6), the transformation is expressed as $\Delta = \tilde{\Delta}\mathbf{P}$, where \mathbf{P} is the projection matrix that suppresses updates within the benign subspace. The steering constraint can thus be formulated as:

$$\Delta\mathbf{H}_m = \tilde{\Delta}\mathbf{P}\mathbf{H}_m = \mathbf{R}, \quad (10)$$

where $\mathbf{R} \in \mathbb{R}^{d \times N_m}$ represents the target refusal activations, each column corresponding to the hidden state when the model generates a safe refusal for the same adversarial image under different queries. The basic objective aims to align steered activations with \mathbf{R} while regularizing the transformation magnitude:

$$\tilde{\Delta}^* = \arg \min_{\tilde{\Delta}} \left(\|\tilde{\Delta}\mathbf{P}\mathbf{H}_m - \mathbf{R}\|_F^2 + \alpha \|\tilde{\Delta}\mathbf{P}\|_F^2 \right), \quad (11)$$

where α controls the smoothness of the transformation within the constrained subspace.

To further suppress residual jailbreak semantics, we extract attribution-based harmful directions \mathbf{V} following the same set of malicious activations \mathbf{H}_m . For each sample v in the harmful set \mathcal{D}_m , we mask visually salient tokens and measure the resulting activation change:

$$\delta(v) = \mathbf{h}(v) - \mathbf{h}(\text{Mask}(v)) \in \mathbb{R}^d. \quad (12)$$

Stacking these deltas across all samples yields:

$$\mathbf{V} = [\delta(v_1) \delta(v_2) \cdots \delta(v_{N_m})] \in \mathbb{R}^{d \times N_m}, \quad (13)$$

which captures harmful directions at the steering and serves as the suppression target in the final objective:

$$\tilde{\Delta}^* = \arg \min_{\tilde{\Delta}} \left(\|\tilde{\Delta}\mathbf{P}\mathbf{H}_m - \mathbf{R}\|_F^2 + \alpha \|\tilde{\Delta}\mathbf{P}\|_F^2 + \beta \|\tilde{\Delta}\mathbf{P}\mathbf{H}_m - \mathbf{V}\|_F^2 \right), \quad (14)$$

where β balances the suppression of harmful activation alignment. The second term enforces stability, while the third term explicitly discourages projection onto jailbreak-related directions. The closed-form solution is derived as:

$$\tilde{\Delta}^* = (\mathbf{R} + \beta\mathbf{V})\mathbf{H}_m^\top \mathbf{P}^\top (\mathbf{P}\mathbf{H}_m\mathbf{H}_m^\top \mathbf{P}^\top + (\alpha + \beta)\mathbf{P}\mathbf{P}^\top)^+, \quad (15)$$

where $^+$ denotes the Moore–Penrose pseudoinverse (see the derivation in Section A of the Supplementary). At inference, each hidden activation $\mathbf{h}^{(l)}$ is updated as

$$\mathbf{h}^{(l)'} = \mathbf{h}^{(l)} + \lambda \tilde{\Delta}^{*(l)}\mathbf{P}^{(l)}\mathbf{h}^{(l)}, \quad (16)$$

where λ controls the steering intensity. By combining null-space projection with refusal-oriented transformation,

NullSteer selectively suppresses harmful activations while preserving benign behaviors.

4. Experiments

In this section, we evaluate NullSteer on multimodal safety benchmarks, analyzing its robustness, utility preservation, and the contribution of each component through ablation and visualization.

4.1. Setup

Dataset. We construct test sets for two attack scenarios, *Toxicity* and *Jailbreak*, using perturbation-based adversarial images. Following the data preparation of ASTRA [52], we start from clean images sampled from ImageNet [9] and apply the PGD attack [35] to produce adversarial examples for both steering-vector construction and evaluation. Specifically, 55 benign images are sampled, from which 30 adversarial samples are used for testing, while an additional 16 adversarial images (under the same PGD settings) are generated for steering-vector construction. The perturbation radius is set to $\epsilon \in \{\frac{16}{255}, \frac{32}{255}, \frac{64}{255}, \text{unconstrained}\}$. Details of the PGD configuration are provided in Section B of the Supplementary Material.

For textual prompts, the Toxicity test set contains 100 samples drawn from RealToxicityPrompt [16], while the Jailbreak test set includes 110 prompts sampled from Advbench [72] and Anthropic-HHH [14]. All textual prompts are disjoint from those used in steering-vector construction. We evaluate model utility in benign settings using two widely adopted multimodal reasoning benchmarks, MM-Vet [62] and MM-Bench [32], which cover diverse vision-language understanding and instruction-following tasks. To additionally examine over-refusal behaviors, we include safe instructions from XSTest [46], allowing analysis of whether safety mechanisms affect normal task responses.

Models & Baselines. We conduct experiments on three representative open-source VLMs, including Qwen2-VL-7B [1], MiniGPT-4-13B [66], and LLaVA-v1.5-13B [28]. The steering layer l is set to 20 for 13B models and 14 for 7B models. We follow the experimental settings of previous work [52] for attribution ablation in Eq. (12). For comparison, we include three VLM defense baselines and three steering-based approaches. Among VLM defenses, Self-Reminder [60] introduces safety control via system prompts, JailGuard [4] detects unsafe content by perturbing input images and comparing response divergence, and ECSO [19] converts unsafe visual inputs into text to activate intrinsic safety mechanisms of the underlying LLM. For steering-based defenses, Wang et al. [52] perform adaptive activation steering by deriving transferable vectors from ablated adversarial tokens, and Rimsky et al. [45] with Ball et al. [2] construct textual steering vectors encoding refusal semantics and jailbreak templates.

4.2. Main results

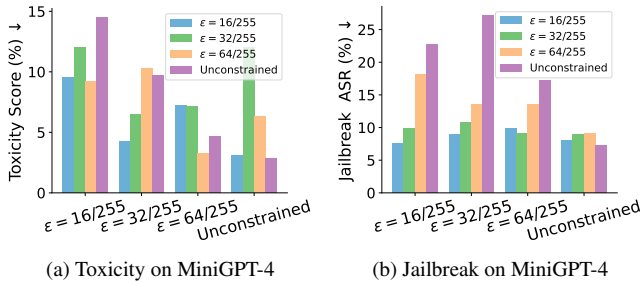
Defense performance. Table 1 reports the defense results under perturbation-based attacks on MiniGPT-4, Qwen2-VL, and LLaVA-v1.5. Across all settings, NullSteer consistently attains the lowest Toxicity Score and ASR, indicating stable robustness and generalization across architectures. Under the strongest unconstrained attack on MiniGPT-4, NullSteer records a Toxicity Score of 2.89% and an ASR of 7.32%, compared with 42.86% and 37.27% from ECSO and 4.48% and 9.09% from ASTRA. Similar trends are observed on Qwen2-VL and LLaVA-v1.5. For Qwen2-VL under $\epsilon=32/255$, NullSteer attains a Toxicity of 3.51% and an ASR of 4.55%, while ASTRA [52] reports 5.45% and 5.00%, respectively. For LLaVA-v1.5 under $\epsilon=32/255$, NullSteer achieves 31.82% Toxicity and 8.75% ASR, compared with 34.76% and 10.91% from ASTRA. Traditional VLM defenses such as Self-Reminder [60], JailGuard [4], and ECSO [19] remain highly vulnerable, typically exhibiting Toxicity above 40% and ASR exceeding 50%, highlighting the limitations of input- or output-level adjustments. In contrast, steering-based defenses provide stronger alignment control, yet Refusal Pairs [44] and Jailbreak Templates [3] show considerably higher Toxicity and ASR due to the lack of multimodal coupling. Compared with ASTRA, NullSteer consistently achieves lower scores across all benchmarks, demonstrating the advantage of null-space-constrained activation steering in enhancing robustness and safety simultaneously.

In the in-distribution (ID) setting, steering vectors are constructed and evaluated on adversarial samples from the same ImageNet classes to assess robustness across perturbation intensities. As shown in Figure 3, NullSteer maintains low Toxicity and Jailbreak scores across varying ϵ levels. The defense derived from $\epsilon = \frac{16}{255}$ remains effective against $\epsilon = \frac{64}{255}$ attacks, with only 7.3% Toxicity and 9.0% Jailbreak. On average, NullSteer achieves 5.78% Toxicity and 3.00% Jailbreak, improving over ASTRA by 4-5%. Overall, these results confirm that NullSteer encodes robust, transferable steering directions that generalize both across and within perturbation distributions. To further validate the generalization of NullSteer beyond in-distribution settings, we additionally perform out-of-distribution (OOD) experiments, with results presented in Section C of the Supplementary Material.

Adaptive attack performance. Adaptive attack assumes the adversary has full knowledge of the defense, including the steering vectors and coefficients. Following this setting, we perform PGD-based adaptive attacks under different perturbation magnitudes. As shown in Figure 4, both ASTRA and our NullSteer reduce Toxicity and Jailbreak scores compared to the undefended baseline. Notably, our NullSteer achieves the lowest Jailbreak rate across all ϵ values, e.g., reducing it from 49.1% to 19.3%

Table 1. Defense comparisons across different VLMs. Lower values (\downarrow) indicate stronger robustness. Steering vectors for each ϵ are derived from adversarial examples generated under the same perturbation level. The best results are highlighted in **bold**.

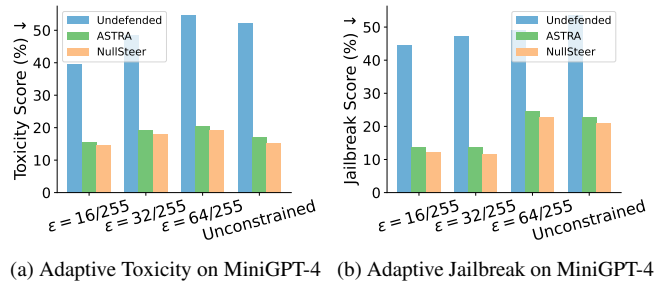
Method		Toxicity (Perturbation-based) – Toxicity Score (%) \downarrow				Jailbreak (Perturbation-based) – ASR (%) \downarrow			
		$\epsilon = 16/255$	$\epsilon = 32/255$	$\epsilon = 64/255$	unconstrained	$\epsilon = 16/255$	$\epsilon = 32/255$	$\epsilon = 64/255$	unconstrained
MiniGPT-4	Benign image	30.65	30.65	30.65	30.65	24.55	24.55	24.55	24.55
	w/o defense	39.73	48.52	54.70	52.12	44.55	47.27	49.09	53.64
	Self-reminder [60]	38.97	48.71	45.15	50.12	35.45	36.36	41.82	43.64
	JailGuard [63]	16.51	18.93	20.93	21.23	30.00	32.73	27.27	28.18
	ECSO [19]	34.59	32.42	38.54	42.86	40.91	42.73	29.09	37.27
	Refusal Pairs [44]	25.76	30.28	31.99	35.71	20.00	22.73	17.27	16.36
	Jailbreak Templates [3]	19.73	25.03	30.10	22.78	33.64	38.15	38.18	42.73
	ASTRA [52]	11.30	8.84	4.51	4.48	9.09	13.18	15.46	9.09
	NullSteer	9.52	6.45	3.26	2.89	7.62	10.72	13.58	7.32
Qwen2-VL	Benign image	38.52	38.52	38.52	38.52	0.00	0.00	0.00	0.00
	w/o defense	50.50	51.62	55.59	53.43	67.27	70.46	71.82	76.36
	Self-reminder [60]	30.47	27.53	32.84	29.09	50.00	47.27	40.00	58.18
	JailGuard [63]	29.37	24.68	28.74	27.76	19.09	20.00	21.82	15.45
	ECSO [19]	50.09	50.68	56.08	51.57	30.00	27.27	31.82	32.73
	Refusal Pairs [44]	46.14	46.83	46.83	40.53	29.09	31.82	21.82	52.73
	Jailbreak Templates [3]	66.74	63.35	67.15	68.29	68.18	68.18	65.45	74.55
	ASTRA [52]	15.52	5.45	2.39	0.07	6.06	5.00	18.18	15.45
	NullSteer	13.36	3.51	1.98	0.05	4.21	4.55	15.82	13.25
LLaVA-v1.5	Benign image	75.00	75.00	75.00	75.00	13.64	13.64	13.64	13.64
	w/o defense	83.70	84.40	85.54	85.44	51.82	56.36	55.45	53.64
	Self-reminder [60]	83.92	83.97	84.19	80.93	28.18	30.00	22.73	22.73
	JailGuard [3]	77.60	77.77	75.76	73.76	23.64	21.82	30.00	17.27
	ECSO [19]	73.77	73.14	71.32	66.81	24.55	21.82	14.55	20.00
	Refusal Pairs [44]	66.72	66.82	60.36	62.46	23.64	25.45	20.00	19.09
	Jailbreak Templates [3]	52.61	50.21	55.48	54.90	23.64	17.27	20.00	29.09
	ASTRA [52]	36.02	34.76	43.13	25.10	4.55	10.91	13.64	12.43
	NullSteer	32.55	31.82	39.32	22.35	3.18	8.75	11.48	10.25



(a) Toxicity on MiniGPT-4

(b) Jailbreak on MiniGPT-4

Figure 3. Transferability performance under ID conditions.



(a) Adaptive Toxicity on MiniGPT-4 (b) Adaptive Jailbreak on MiniGPT-4

Figure 4. Adaptive attack performance on MiniGPT-4.

at $\epsilon = \frac{64}{255}$. These results demonstrate that NullSteer maintains strong robustness even when the attacker optimizes against the defense, validating its stability under the most challenging white-box setting.

Utility performance. Table 2 compares the utility of defended models under benign and adversarial conditions. Across MM-Vet, MMBench, and XSTest, NullSteer maintains comparable or higher utility scores than AS-

TRA and Vanilla models, indicating that our defense does not compromise benign performance. For instance, on MiniGPT-4, the MM-Vet score slightly improves from 19.40 to 21.05, and similar trends are observed on Qwen2-VL and LLaVA-v1.5. Under adversarial scenarios, NullSteer consistently achieves the lowest perplexity, confirming its ability to produce coherent and safe outputs when facing harmful prompts. On MiniGPT-4, the toxicity

Table 2. Utility performance in benign and adversarial scenarios.

Methods		Benign Scenarios – Utility Score \uparrow			Adversarial Scenarios – Perplexity \downarrow		
		MM-Vet [62]	MMBench [32]	XSTest [46]	Toxicity (Perturbation-based)	Jailbreak (Perturbation-based)	Jailbreak (Structured-based)
MiniGPT-4	Vanilla	19.40	35.90	87.60	51.42	3.95	2.62
	ASTRA [52]	20.62	35.82	87.60	10.14	5.82	4.29
	NullSteer	21.05	36.25	87.80	9.52	2.58	3.65
LLaVA-v1.5	Vanilla	32.62	72.94	98.00	63.68	3.68	3.82
	ASTRA [52]	30.55	73.23	98.80	59.28	8.59	4.61
	NullSteer	31.20	73.56	98.80	57.96	7.23	4.26
Qwen2-VL	Vanilla	49.13	78.00	73.60	140.44	6.80	30.00
	ASTRA [52]	48.66	78.69	74.00	40.14	8.86	30.92
	NullSteer	49.02	78.82	74.50	38.45	6.95	30.48

perplexity drops from 51.42 to 9.52, and the jailbreak perplexity from 3.95 to 2.58, demonstrating strong robustness without degrading response quality. This balance between safety and utility stems from the adaptive steering mechanism, which modulates activation shifts in proportion to semantic deviation, preventing over-suppression of normal responses while effectively reducing harmful generation.

4.3. Ablation study

Objective function analysis. We analyze the contribution of the three loss components in Eq. (14): the smoothness regularization $\|\hat{\Delta}\mathbf{P}\|_F^2$, the refusal alignment $\|\hat{\Delta}\mathbf{P}\mathbf{H}_m - \mathbf{R}\|_F^2$, and the harmful suppression $\|\hat{\Delta}\mathbf{P}\mathbf{H}_m - \mathbf{V}\|_F^2$. As shown in Table 3, under the unconstrained perturbation setting on MiniGPT-4, removing any term notably weakens the defense, confirming their complementary effects. The refusal-alignment term provides the dominant safety improvement by steering harmful activations toward refusal semantics, while the harmful-suppression term further reduces residual correlations with jailbreak features, enhancing robustness under strong perturbations. The smoothness regularization constrains transformation magnitude, ensuring stability in benign subspaces and preserving high utility. When all three objectives are combined, NullSteer attains the lowest Toxicity (2.89%) and ASR (7.32%) with the highest MMBench score (36.25), achieving a balanced trade-off between safety and utility.

Analysis of the number of benign activations. As shown in Figure 5, increasing the number of benign activations N_b used to estimate the null space consistently improves model utility on both MM-VET and MMBench under the unconstrained perturbation setting. When N_b is small, the estimated null space is under-constrained, leading to minor degradation in benign performance. As N_b increases, the projection matrix becomes more stable and accurately captures the invariant subspace of benign activations, resulting in steady utility gains for both MiniGPT-4 and LLaVA-v1.5.

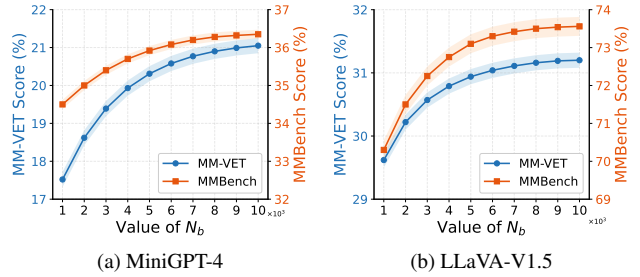


Figure 5. Utility with varying numbers of benign activations N_b . Evaluation is conducted on MM-VET and MMBench with MiniGPT-4 and LLaVA-v1.5 under the unconstrained.

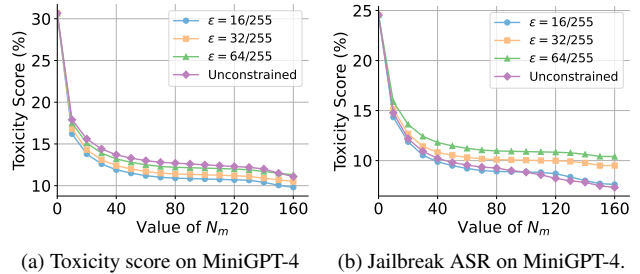


Figure 6. Safety with varying numbers of malicious activations N_m . Evaluation is conducted on MiniGPT-4 under multiple perturbation levels.

The improvement gradually saturates around $N_b \approx 8$, indicating that only a moderate number of benign samples is sufficient to construct a well-conditioned projection without additional computation overhead.

Analysis of the number of malicious activations. As shown in Figure 6, increasing the number of malicious activations N_m used to estimate harmful directions improves the defense effectiveness across all perturbation levels. When N_m is small, the estimated harmful subspace

Table 3. Ablation study of different objective components on MiniGPT-4.

$\ \tilde{\Delta}\mathbf{P}\ _F^2$	$\ \tilde{\Delta}\mathbf{P}\mathbf{H}_m - \mathbf{R}\ _F^2$	$\ \tilde{\Delta}\mathbf{P}\mathbf{H}_m - \mathbf{V}\ _F^2$	Toxicity Score ↓	Jailbreak (ASR) ↓	Utility Score ↑
✗	✗	✗	30.65	34.55	35.90
✓	✓	✗	3.58	8.36	36.00
✓	✗	✓	4.02	8.57	36.00
✓	✓	✓	2.89	7.32	36.25

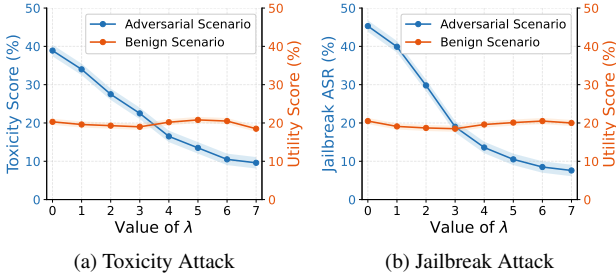


Figure 7. Effect of steering strength on MiniGPT-4. We vary λ when applying activation steering under the $\epsilon = 16/255$ perturbation setting and report Toxicity Score on the Toxicity attack, Jailbreak ASR on the Jailbreak attack, and utility on MM-Vet.

fails to capture consistent jailbreak semantics, leading to higher Toxicity and ASR. As N_m increases, both metrics rapidly decline and stabilize, suggesting that richer harmful evidence enables more reliable direction estimation. Beyond $N_m \approx 100$, the performance gain becomes marginal, indicating that a moderate number of malicious samples is sufficient for efficient steering vector construction.

Analysis of steering strength. Figure 7 illustrates that increasing the steering strength λ progressively suppresses unsafe behaviors on MiniGPT-4. Both Toxicity and Jailbreak ASR drop markedly as λ grows, confirming that stronger activation modulation enhances refusal robustness under adversarial perturbations. The MM-Vet utility remains stable across all settings, demonstrating that steering primarily affects adversarial directions while preserving benign representations. An intermediate strength ($\lambda \approx 5$) yields the best safety–utility balance.

Inference time. Table 4 compares the average decoding latency of different defenses. NullSteer maintains comparable inference speed to the original models, requiring 173.57 ms/token on MiniGPT-4, 40.68 ms/token on LLaVA-v1.5, and 27.66 ms/token on Qwen2-VL. Its average latency of 8.43 shows negligible overhead compared with the undefended models. In contrast, multi-round or auxiliary-based defenses such as JailGuard and ECSO introduce substantial delays, exceeding 1.5 s/token and 450 ms/token, respectively. Compared with the ASTRA, NullSteer achieves slightly lower latency while maintaining robustness, showing its efficiency and practi-

Table 4. Inference time per token (ms). Average decoding latency is computed and normalized by the number of generated tokens. Reporting time per token enables a fair comparison of inference efficiency across models with varying output lengths. Lower values indicate faster decoding.

	MiniGPT-4	LLaVA-v1.5	Qwen2-VL	Avg.
w/o defense	173.19	40.68	27.43	63.67
Self-reminder [60]	173.36	41.09	27.94	53.38
JailGuard [3]	1557.98	366.02	245.42	40.92
ECSO [19]	457.55	116.44	70.22	53.75
ASTRA [52]	173.77	40.69	27.98	9.88
NullSteer	173.57	40.68	27.66	8.43

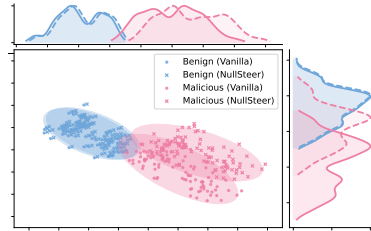


Figure 8. Visualization of activation distributions.

cality for real-time deployment.

Activation distribution analysis. Figure 8 visualizes the activations distributions of benign and malicious inputs before and after applying NullSteer on MiniGPT-4. The benign clusters remain well aligned with the original representations, indicating that our null-space constraint effectively preserves utility by preventing changes in safe directions. In contrast, the malicious activations exhibit a clear displacement toward the refusal region, confirming that NullSteer adaptively redirects unsafe semantics. More visualization results are provided in Section C of the Supplementary Material.

5. Conclusion

In this work, We presented NullSteer, a principled activation-steering framework that enhances the safety of vision–language models through null-space–constrained representation modulation. By restricting steering to direc-

tions orthogonal to benign activations, NullSteer preserves normal behavior while effectively suppressing unsafe semantics. Extensive evaluations demonstrate its superior robustness under both perturbation-based and adaptive attacks without compromising utility. Our study highlights the potential of representation-level alignment as a general and efficient paradigm for building safe and reliable multi-modal large language models. Future work will explore extending null-space steering to larger-scale alignment tasks and integrating it with adaptive safety tuning during fine-tuning or instruction following.

Acknowledge

This research is supported by the National Natural Science Foundation of China (No.U24B20180, No. 62576330) and National Natural Science Foundation of Anhui (No.2508085MF143).

References

- [1] Jinze Bai, Shuai Bai, Shusheng Yang, Shijie Wang, Sinan Tan, Peng Wang, Junyang Lin, Chang Zhou, and Jingren Zhou. Qwen-vl: A frontier large vision-language model with versatile abilities. *CoRR*, abs/2308.12966, 2023. 5, 1
- [2] Sarah Ball, Frauke Kreuter, and Nina Rimsky. Understanding jailbreak success: A study of latent space dynamics in large language models. *CoRR*, abs/2406.09289, 2024. 5
- [3] Sarah Ball, Frauke Kreuter, and Nina Rimsky. Understanding jailbreak success: A study of latent space dynamics in large language models. *CoRR*, abs/2406.09289, 2024. 5, 6, 8
- [4] Patrick Chao, Edoardo DeBenedetti, Alexander Robey, Maksym Andriushchenko, Francesco Croce, Vikash Sehwal, Edgar Dobriban, Nicolas Flammarion, George J. Pappas, Florian Tramèr, Hamed Hassani, and Eric Wong. Jailbreakbench: An open robustness benchmark for jailbreaking large language models. In *NeurIPS*, 2024. 5
- [5] Jun Chen, Deyao Zhu, Xiaoqian Shen, Xiang Li, Zechun Liu, Pengchuan Zhang, Raghuraman Krishnamoorthi, Vikas Chandra, Yunyang Xiong, and Mohamed Elhoseiny. Minigt-v2: large language model as a unified interface for vision-language multi-task learning. *CoRR*, abs/2310.09478, 2023. 1
- [6] Yangyi Chen, Karan Sikka, Michael Cogswell, Heng Ji, and Ajay Divakaran. DRESS : Instructing large vision-language models to align and interact with humans via natural language feedback. In *CVPR*, 2024. 2
- [7] Francesco Croce and Matthias Hein. Reliable evaluation of adversarial robustness with an ensemble of diverse parameter-free attacks. In *ICML*, 2020. 2
- [8] Wenliang Dai, Junnan Li, Dongxu Li, Anthony Meng Huat Tiong, Junqi Zhao, Weisheng Wang, Boyang Li, Pascale Fung, and Steven C. H. Hoi. Instructblip: Towards general-purpose vision-language models with instruction tuning. In *NeurIPS*, 2023. 1
- [9] Jia Deng, Wei Dong, Richard Socher, Li-Jia Li, Kai Li, and Li Fei-Fei. Imagenet: A large-scale hierarchical image database. In *CVPR*, 2009. 5
- [10] Yi Ding, Bolian Li, and Ruqi Zhang. ETA: evaluating then aligning safety of vision language models at inference time. In *ICLR*, 2025. 2
- [11] Yinpeng Dong, Fangzhou Liao, Tianyu Pang, Hang Su, Jun Zhu, Xiaolin Hu, and Jianguo Li. Boosting adversarial attacks with momentum. In *CVPR*, 2018. 2
- [12] Junfeng Fang, Shuai Zhang, Chang Wu, Zhengyi Yang, Zhiyuan Liu, Sihang Li, Kun Wang, Wenjie Du, and Xiang Wang. Molc: Towards molecular relational modeling in language models. In *ACL (Findings)*, 2024. 2
- [13] Junfeng Fang, Houcheng Jiang, Kun Wang, Yunshan Ma, Jie Shi, Xiang Wang, Xiangnan He, and Tat-Seng Chua. Alphaedit: Null-space constrained knowledge editing for language models. In *ICLR*, 2025. 2, 3
- [14] Deep Ganguli, Liane Lovitt, Jackson Kernion, Amanda Askell, Yuntao Bai, Saurav Kadavath, Ben Mann, Ethan Perez, Nicholas Schiefer, Kamal Ndousse, Andy Jones, Sam Bowman, Anna Chen, Tom Conerly, Nova DasSarma, Dawn Drain, Nelson Elhage, Sheer El Showk, Stanislav Fort, Zac Hatfield-Dodds, Tom Henighan, Danny Hernandez, Tristan Hume, Josh Jacobson, Scott Johnston, Shauna Kravec, Catherine Olsson, Sam Ringer, Eli Tran-Johnson, Dario Amodei, Tom Brown, Nicholas Joseph, Sam McCandlish, Chris Olah, Jared Kaplan, and Jack Clark. Red teaming language models to reduce harms: Methods, scaling behaviors, and lessons learned. *CoRR*, abs/2209.07858, 2022. 5
- [15] Jiahui Gao, Renjie Pi, Tianyang Han, Han Wu, Lanqing Hong, Lingpeng Kong, Xin Jiang, and Zhenguo Li. Coca: Regaining safety-awareness of multimodal large language models with constitutional calibration. *CoRR*, abs/2409.11365, 2024. 2
- [16] Samuel Gehman, Suchin Gururangan, Maarten Sap, Yejin Choi, and Noah A. Smith. Realtocixityprompts: Evaluating neural toxic degeneration in language models. In *EMNLP (Findings)*, 2020. 5
- [17] Soumya Suvra Ghosal, Souradip Chakraborty, Vaibhav Singh, Tianrui Guan, Mengdi Wang, Ahmad Beirami, Furong Huang, Alvaro Velasquez, Dinesh Manocha, and Amrit Singh Bedi. Immune: Improving safety against jailbreaks in multi-modal llms via inference-time alignment. In *CVPR*, 2025. 1, 2
- [18] Yichen Gong, Delong Ran, Jinyuan Liu, Conglei Wang, Tianshuo Cong, Anyu Wang, Sisi Duan, and Xiaoyun Wang. Figstep: Jailbreaking large vision-language models via typographic visual prompts. In *AAAI*, 2025. 1, 2
- [19] Yunhao Gou, Kai Chen, Zhili Liu, Lanqing Hong, Hang Xu, Zhenguo Li, Dit-Yan Yeung, James T. Kwok, and Yu Zhang. Eyes closed, safety on: Protecting multimodal llms via image-to-text transformation. In *ECCV*, 2024. 1, 5, 6, 8
- [20] Dongchen Han, Xiaojun Jia, Yang Bai, Jindong Gu, Yang Liu, and Xiaochun Cao. Ot-attack: Enhancing adversarial transferability of vision-language models via optimal transport optimization. *CoRR*, abs/2312.04403, 2023. 1
- [21] Yue Huang, Lichao Sun, Haoran Wang, Siyuan Wu, Qihui Zhang, Yuan Li, Chujie Gao, Yixin Huang, Wenhan Lyu,

- Yixuan Zhang, Xiner Li, Hanchi Sun, Zhengliang Liu, Yixin Liu, Yijue Wang, Zhikun Zhang, Bertie Vidgen, Bhavya Kailkhura, Caiming Xiong, Chaowei Xiao, Chunyuan Li, Eric P. Xing, Furong Huang, Hao Liu, Heng Ji, Hongyi Wang, Huan Zhang, Huaxiu Yao, Manolis Kellis, Marinka Zitnik, Meng Jiang, Mohit Bansal, James Zou, Jian Pei, Jian Liu, Jianfeng Gao, Jiawei Han, Jieyu Zhao, Jiliang Tang, Jindong Wang, Joaquin Vanschoren, John C. Mitchell, Kai Shu, Kaidi Xu, Kai-Wei Chang, Lifang He, Lifu Huang, Michael Backes, Neil Zhenqiang Gong, Philip S. Yu, Pin-Yu Chen, Quanquan Gu, Ran Xu, Rex Ying, Shuiwang Ji, Suman Jana, Tianlong Chen, Tianming Liu, Tianyi Zhou, William Wang, Xiang Li, Xiangliang Zhang, Xiao Wang, Xing Xie, Xun Chen, Xuyi Wang, Yan Liu, Yanfang Ye, Yinzhi Cao, Yong Chen, and Yue Zhao. Position: Trustllm: Trustworthiness in large language models. In *ICML*, 2024. 1
- [22] Houcheng Jiang, Junfeng Fang, Ningyu Zhang, Mingyang Wan, Guojun Ma, Xiang Wang, Xiangnan He, and Tat-Seng Chua. Anyedit: Edit any knowledge encoded in language models. In *ICML*, 2025. 2
- [23] Maxim Khanov, Jirayu Burapachep, and Yixuan Li. ARGS: alignment as reward-guided search. In *ICLR*, 2024. 2
- [24] Alexey Kurakin, Ian J. Goodfellow, and Samy Bengio. Adversarial machine learning at scale. In *ICLR*, 2017. 1
- [25] Mukai Li, Lei Li, Yuwei Yin, Masood Ahmed, Zhenguang Liu, and Qi Liu. Red teaming visual language models. In *ACL (Findings)*, 2024. 1, 2
- [26] Huawei Lin, Yingjie Lao, Tong Geng, Tan Yu, and Weijie Zhao. Uniguardian: A unified defense for detecting prompt injection, backdoor attacks and adversarial attacks in large language models. *CoRR*, abs/2502.13141, 2025. 2
- [27] Haotian Liu, Chunyuan Li, Qingyang Wu, and Yong Jae Lee. Visual instruction tuning. In *NeurIPS*, 2023. 1
- [28] Haotian Liu, Chunyuan Li, Qingyang Wu, and Yong Jae Lee. Visual instruction tuning. In *NeurIPS*, 2023. 5, 1
- [29] Sheng Liu, Haotian Ye, and James Zou. Reducing hallucinations in large vision-language models via latent space steering. In *ICLR*, 2025. 2
- [30] Xin Liu, Yichen Zhu, Yunshi Lan, Chao Yang, and Yu Qiao. Query-relevant images jailbreak large multi-modal models. *CoRR*, abs/2311.17600, 2023. 1
- [31] Xin Liu, Yichen Zhu, Jindong Gu, Yunshi Lan, Chao Yang, and Yu Qiao. Mm-safetybench: A benchmark for safety evaluation of multimodal large language models. In *ECCV*, 2024. 2
- [32] Yuan Liu, Haodong Duan, Yuanhan Zhang, Bo Li, Songyang Zhang, Wangbo Zhao, Yike Yuan, Jiaqi Wang, Conghui He, Ziwei Liu, Kai Chen, and Dahua Lin. Mmbench: Is your multi-modal model an all-around player? In *ECCV*, 2024. 5, 7
- [33] Yuheng Lu, Bingshuo Qian, Caixia Yuan, Huixing Jiang, and Xiaojie Wang. Controlled low-rank adaptation with subspace regularization for continued training on large language models. In *ACL*, 2025. 2
- [34] Aleksander Madry, Aleksandar Makelov, Ludwig Schmidt, Dimitris Tsipras, and Adrian Vladu. Towards deep learning models resistant to adversarial attacks. In *ICLR*, 2018. 2
- [35] Aleksander Madry, Aleksandar Makelov, Ludwig Schmidt, Dimitris Tsipras, and Adrian Vladu. Towards deep learning models resistant to adversarial attacks. In *ICLR*, 2018. 5
- [36] Mantas Mazeika, Long Phan, Xuwang Yin, Andy Zou, Zifan Wang, Norman Mu, Elham Sakhae, Nathaniel Li, Steven Basart, Bo Li, David A. Forsyth, and Dan Hendrycks. Harmbench: A standardized evaluation framework for automated red teaming and robust refusal. In *ICML*, 2024. 2
- [37] Sidharth Mudgal, Jong Lee, Harish Ganapathy, YaGuang Li, Tao Wang, Yanping Huang, Zhifeng Chen, Heng-Tze Cheng, Michael Collins, Trevor Strohman, Jilin Chen, Alex Beutel, and Ahmad Beirami. Controlled decoding from language models. In *ICML*, 2024. 2
- [38] Yi Nian, Shenzhe Zhu, Yuehan Qin, Li Li, Ziyi Wang, Chaowei Xiao, and Yue Zhao. Jaildam: Jailbreak detection with adaptive memory for vision-language model. *CoRR*, abs/2504.03770, 2025. 1
- [39] Yuji Okamoto and Ryosuke Kojima. Learning deep dissipative dynamics. In *AAAI*, 2025. 2
- [40] Tiantian Peng, Yuyang Liu, Shuo Yang, Qiuhe Hong, and Yonghong Tian. GNSP: gradient null space projection for preserving cross-modal alignment in vlms continual learning. *CoRR*, abs/2507.19839, 2025. 2
- [41] Renjie Pi, Tianyang Han, Jianshu Zhang, Yueqi Xie, Rui Pan, Qing Lian, Hanze Dong, Jipeng Zhang, and Tong Zhang. Mllm-protector: Ensuring mllm’s safety without hurting performance. In *EMNLP*, 2024. 1
- [42] Xiangyu Qi, Kaixuan Huang, Ashwinee Panda, Peter Henderson, Mengdi Wang, and Prateek Mittal. Visual adversarial examples jailbreak aligned large language models. In *AAAI*, 2024. 1
- [43] Zihuan Qiu, Lei Wang, Yang Cao, Runtong Zhang, Bing Su, Yi Xu, Fanman Meng, Linfeng Xu, Qingbo Wu, and Hongliang Li. Null-space filtering for data-free continual model merging: Preserving transparency, promoting fidelity. *CoRR*, abs/2509.21413, 2025. 2
- [44] Nina Rimskey, Nick Gabrieli, Julian Schulz, Meg Tong, Evan Hubinger, and Alexander Matt Turner. Steering llama 2 via contrastive activation addition. In *ACL*, 2024. 5, 6
- [45] Nina Rimskey, Nick Gabrieli, Julian Schulz, Meg Tong, Evan Hubinger, and Alexander Matt Turner. Steering llama 2 via contrastive activation addition. In *ACL*, 2024. 5
- [46] Paul Röttger, Hannah Kirk, Bertie Vidgen, Giuseppe Attanasio, Federico Bianchi, and Dirk Hovy. Xstest: A test suite for identifying exaggerated safety behaviours in large language models. In *NAACL-HLT*, 2024. 5, 7
- [47] Rylan Schaeffer, Dan Valentine, Luke Bailey, James Chua, Cristóbal Eyzaguirre, Zane Durante, Joe Benton, Brando Miranda, Henry Sleight, John Hughes, Rajashree Agrawal, Mrinank Sharma, Scott Emmons, Sanmi Koyejo, and Ethan Perez. When do universal image jailbreaks transfer between vision-language models? *CoRR*, abs/2407.15211, 2024. 1
- [48] Christian Schlarmann and Matthias Hein. On the adversarial robustness of multi-modal foundation models. In *ICCV (Workshops)*, 2023. 1
- [49] Erfan Shayegani, Yue Dong, and Nael B. Abu-Ghazaleh. Jailbreak in pieces: Compositional adversarial attacks on multi-modal language models. In *ICLR*, 2024. 1

- [50] Leheng Sheng, Changshuo Shen, Weixiang Zhao, Junfeng Fang, Xiaohao Liu, Zhenkai Liang, Xiang Wang, An Zhang, and Tat-Seng Chua. Alphasteer: Learning refusal steering with principled null-space constraint. *CoRR*, abs/2506.07022, 2025. 2, 3
- [51] Boxin Wang, Weixin Chen, Hengzhi Pei, Chulin Xie, Mintong Kang, Chenhui Zhang, Chejian Xu, Zidi Xiong, Ritik Dutta, Rylan Schaeffer, Sang T. Truong, Simran Arora, Mantas Mazeika, Dan Hendrycks, Zinan Lin, Yu Cheng, Sanmi Koyejo, Dawn Song, and Bo Li. Decodingtrust: A comprehensive assessment of trustworthiness in GPT models. In *NeurIPS*, 2023. 1
- [52] Han Wang, Gang Wang, and Huan Zhang. Steering away from harm: An adaptive approach to defending vision language model against jailbreaks. In *CVPR*, pages 29947–29957. Computer Vision Foundation / IEEE, 2025. 2, 5, 6, 7, 8
- [53] Ruipeng Wang, Junfeng Fang, Jiaqi Li, Hao Chen, Jie Shi, Kun Wang, and Xiang Wang. ACE: concept editing in diffusion models without performance degradation. *CoRR*, abs/2503.08116, 2025. 2
- [54] Shipeng Wang, Xiaorong Li, Jian Sun, and Zongben Xu. Training networks in null space of feature covariance for continual learning. In *CVPR*, 2021. 2, 3
- [55] Yinhuai Wang, Jiwen Yu, and Jian Zhang. Zero-shot image restoration using denoising diffusion null-space model. In *ICLR*, 2023. 2
- [56] Yu Wang, Xiaogeng Liu, Yu Li, Muhao Chen, and Chaowei Xiao. Adashield: Safeguarding multimodal large language models from structure-based attack via adaptive shield prompting. In *ECCV*, 2024. 1, 2
- [57] Lyucheng Wu, Mengru Wang, Ziwen Xu, Tri Cao, Nay Oo, Bryan Hooi, and Shumin Deng. Automating steering for safe multimodal large language models. *CoRR*, abs/2507.13255, 2025. 2
- [58] Yongliang Wu, Xinting Hu, Yuyang Sun, Yizhou Zhou, Wenbo Zhu, Fengyun Rao, Bernt Schiele, and Xu Yang. Number it: Temporal grounding videos like flipping manga. In *CVPR*, 2025. 1
- [59] Yongliang Wu, Yizhou Zhou, Zhou Ziheng, Yingzhe Peng, Xinyu Ye, Xinting Hu, Wenbo Zhu, Lu Qi, Ming-Hsuan Yang, and Xu Yang. On the generalization of sft: A reinforcement learning perspective with reward rectification. *arXiv preprint arXiv:2508.05629*, 2025. 1
- [60] Yueqi Xie, Jingwei Yi, Jiawei Shao, Justin Curl, Lingjuan Lyu, Qifeng Chen, Xing Xie, and Fangzhao Wu. Defending chatgpt against jailbreak attack via self-reminders. *Nat. Mac. Intell.*, 5(12):1486–1496, 2023. 5, 6, 8
- [61] Jiazhen Yan, Fan Wang, Weiwei Jiang, Ziqiang Li, and Zhangjie Fu. Ns-net: Decoupling CLIP semantic information through null-space for generalizable ai-generated image detection. *CoRR*, abs/2508.01248, 2025. 2
- [62] Weihao Yu, Zhengyuan Yang, Linjie Li, Jianfeng Wang, Kevin Lin, Zicheng Liu, Xinchao Wang, and Lijuan Wang. Mm-vet: Evaluating large multimodal models for integrated capabilities. In *ICML*, 2024. 5, 7
- [63] Xiaoyu Zhang, Cen Zhang, Tianlin Li, Yihao Huang, Xiaojun Jia, Xiaofei Xie, Yang Liu, and Chao Shen. A mutation-based method for multi-modal jailbreaking attack detection. *CoRR*, abs/2312.10766, 2023. 6
- [64] Jiaqi Zhao, Miao Zhang, Weili Guan, and Liqiang Nie. Boost post-training quantization via null space optimization for large language models. *CoRR*, abs/2506.11044, 2025. 2
- [65] Xuandong Zhao, Xianjun Yang, Tianyu Pang, Chao Du, Lei Li, Yu-Xiang Wang, and William Yang Wang. Weak-to-strong jailbreaking on large language models. *CoRR*, abs/2401.17256, 2024. 1
- [66] Deyao Zhu, Jun Chen, Xiaoqian Shen, Xiang Li, and Mohamed Elhoseiny. Minigpt-4: Enhancing vision-language understanding with advanced large language models. In *ICLR*, 2024. 1, 5
- [67] Xingyu Zhu, Beier Zhu, Yi Tan, Shuo Wang, Yanbin Hao, and Hanwang Zhang. Enhancing zero-shot vision models by label-free prompt distribution learning and bias correcting. In *NeurIPS*, 2024.
- [68] Xingyu Zhu, Shuo Wang, Beier Zhu, Miaoge Li, Yunfan Li, Junfeng Fang, Zhicai Wang, Dongsheng Wang, and Hanwang Zhang. Dynamic multimodal prototype learning in vision-language models. *CoRR*, abs/2507.03657, 2025. 1
- [69] Xingyu Zhu, Kesen Zhao, Liang Yi, Shuo Wang, Zhicai Wang, Beier Zhu, Hanwang Zhang, and Xiangnan He. Look carefully: Adaptive visual reinforcements in multimodal large language models for hallucination mitigation. In *ICLR*, 2026. 2
- [70] Xingyu Zhu, Beier Zhu, Junfeng Fang, Shuo Wang, Yin Zhang, Xiang Wang, and Xiangnan He. Guardalign: Test-time safety alignment in multimodal large language models. In *ICLR*, 2026. 1
- [71] Yongshuo Zong, Ondrej Bohdal, Tingyang Yu, Yongxin Yang, and Timothy M. Hospedales. Safety fine-tuning at (almost) no cost: A baseline for vision large language models. In *ICML*, 2024. 2
- [72] Andy Zou, Zifan Wang, J. Zico Kolter, and Matt Fredrikson. Universal and transferable adversarial attacks on aligned language models. *CoRR*, abs/2307.15043, 2023. 2, 5

A. Derivation of Eq. (7) and Eq. (15)

A.1. Eq. (7): Null-space equivalence

Let $\mathbf{H}_b \in \mathbb{R}^{d \times N_b}$ be the benign activation matrix. Eq. (7) claims that the left null space of \mathbf{H}_b coincides with that of its Gram matrix:

$$\text{Null}(\mathbf{H}_b) = \text{Null}(\mathbf{H}_b \mathbf{H}_b^\top). \quad (17)$$

The null spaces are defined by:

$$\text{Null}(\mathbf{H}_b) = \{\mathbf{x} \in \mathbb{R}^d : \mathbf{x}^\top \mathbf{H}_b = \mathbf{0}^\top\}, \quad (18)$$

$$\text{Null}(\mathbf{H}_b \mathbf{H}_b^\top) = \{\mathbf{x} \in \mathbb{R}^d : \mathbf{x}^\top \mathbf{H}_b \mathbf{H}_b^\top = \mathbf{0}^\top\}. \quad (19)$$

To show the inclusion $\text{Null}(\mathbf{H}_b) \subseteq \text{Null}(\mathbf{H}_b \mathbf{H}_b^\top)$, take any \mathbf{x} such that $\mathbf{x}^\top \mathbf{H}_b = \mathbf{0}^\top$. Using this condition:

$$\mathbf{x}^\top \mathbf{H}_b \mathbf{H}_b^\top = (\mathbf{x}^\top \mathbf{H}_b) \mathbf{H}_b^\top = \mathbf{0}^\top, \quad (20)$$

which confirms $\mathbf{x} \in \text{Null}(\mathbf{H}_b \mathbf{H}_b^\top)$. Conversely, assume $\mathbf{x}^\top \mathbf{H}_b \mathbf{H}_b^\top = \mathbf{0}^\top$. Since $\mathbf{H}_b \mathbf{H}_b^\top$ is symmetric and positive semidefinite, its quadratic form satisfies:

$$\mathbf{x}^\top \mathbf{H}_b \mathbf{H}_b^\top \mathbf{x} = \|\mathbf{H}_b^\top \mathbf{x}\|_2^2 \geq 0. \quad (21)$$

Multiplying the nullity condition by \mathbf{x} yields:

$$0 = \mathbf{x}^\top \mathbf{H}_b \mathbf{H}_b^\top \mathbf{x} = \|\mathbf{H}_b^\top \mathbf{x}\|_2^2, \quad (22)$$

which forces $\mathbf{H}_b^\top \mathbf{x} = \mathbf{0}$ and thus $\mathbf{x}^\top \mathbf{H}_b = \mathbf{0}^\top$. Hence $\mathbf{x} \in \text{Null}(\mathbf{H}_b)$. Since each null space is contained in the other, the equivalence in Eq. (17) follows:

$$\text{Null}(\mathbf{H}_b) = \text{Null}(\mathbf{H}_b \mathbf{H}_b^\top). \quad (23)$$

A.2. Closed-form Solution of Eq. (15)

We derive the closed-form solution of the regularized least-squares problem in Eq. (14). Recall that the objective is:

$$\begin{aligned} \tilde{\Delta}^* = \arg \min_{\tilde{\Delta}} & \left(\|\tilde{\Delta} \mathbf{P} \mathbf{H}_m - \mathbf{R}\|_F^2 \right. \\ & \left. + \alpha \|\tilde{\Delta} \mathbf{P}\|_F^2 + \beta \|\tilde{\Delta} \mathbf{P} \mathbf{H}_m - \mathbf{V}\|_F^2 \right), \\ & \alpha > 0, \beta \geq 0. \end{aligned}$$

For notational simplicity, we introduce:

$$\begin{aligned} \mathbf{X} &:= \mathbf{P} \mathbf{H}_m \in \mathbb{R}^{d \times N_m}, \\ \mathbf{Z} &:= \mathbf{P} \in \mathbb{R}^{d \times d}, \\ \mathbf{Y} &:= \mathbf{R} + \beta \mathbf{V} \in \mathbb{R}^{d \times N_m}, \\ \mathbf{W} &:= \tilde{\Delta} \in \mathbb{R}^{d \times d}. \end{aligned} \quad (24)$$

Grouping the two alignment terms in (A.2), the objective can be written in the compact form:

$$J(\mathbf{W}) = \|\mathbf{W} \mathbf{X} - \mathbf{Y}\|_F^2 + (\alpha + \beta) \|\mathbf{W} \mathbf{Z}\|_F^2, \quad (25)$$

which corresponds to a matrix-valued ridge regression with effective target \mathbf{Y} and regularization coefficient $\alpha + \beta$.

Using $\|\mathbf{A}\|_F^2 = \text{tr}(\mathbf{A} \mathbf{A}^\top)$, we expand (25) in trace form:

$$\begin{aligned} J(\mathbf{W}) = \text{tr} & [(\mathbf{W} \mathbf{X} - \mathbf{Y})(\mathbf{W} \mathbf{X} - \mathbf{Y})^\top] \\ & + (\alpha + \beta) \text{tr}[(\mathbf{W} \mathbf{Z})(\mathbf{W} \mathbf{Z})^\top]. \end{aligned} \quad (26)$$

Taking the derivative with respect to \mathbf{W} and using the standard rule:

$$\nabla_{\mathbf{W}} \text{tr}(\mathbf{W} \mathbf{A} \mathbf{W}^\top \mathbf{B}) = 2 \mathbf{B} \mathbf{W} \mathbf{A}, \quad (27)$$

we obtain the gradient:

$$\nabla_{\mathbf{W}} J = 2(\mathbf{W} \mathbf{X} - \mathbf{Y}) \mathbf{X}^\top + 2(\alpha + \beta) \mathbf{W} \mathbf{Z} \mathbf{Z}^\top. \quad (28)$$

Setting $\nabla_{\mathbf{W}} J = \mathbf{0}$ yields the stationarity condition:

$$(\mathbf{W} \mathbf{X} - \mathbf{Y}) \mathbf{X}^\top + (\alpha + \beta) \mathbf{W} \mathbf{Z} \mathbf{Z}^\top = \mathbf{0}, \quad (29)$$

which can be rearranged into the linear matrix equation:

$$\mathbf{W} (\mathbf{X} \mathbf{X}^\top + (\alpha + \beta) \mathbf{Z} \mathbf{Z}^\top) = \mathbf{Y} \mathbf{X}^\top. \quad (30)$$

The matrix in parentheses may be rank-deficient because $\mathbf{Z} = \mathbf{P}$ is a projection. We therefore adopt the Moore–Penrose pseudoinverse and obtain the minimum-norm solution:

$$\mathbf{W}^* = \mathbf{Y} \mathbf{X}^\top (\mathbf{X} \mathbf{X}^\top + (\alpha + \beta) \mathbf{Z} \mathbf{Z}^\top)^+. \quad (31)$$

Substituting back $\mathbf{X} = \mathbf{P} \mathbf{H}_m$, $\mathbf{Z} = \mathbf{P}$, $\mathbf{Y} = \mathbf{R} + \beta \mathbf{V}$, and $\mathbf{W} = \tilde{\Delta}$ into (31) gives:

$$\tilde{\Delta}^* = (\mathbf{R} + \beta \mathbf{V}) \mathbf{H}_m^\top \mathbf{P}^\top \left(\mathbf{P} \mathbf{H}_m \mathbf{H}_m^\top \mathbf{P}^\top + (\alpha + \beta) \mathbf{P} \mathbf{P}^\top \right)^+, \quad (32)$$

which coincides with Eq. (15) in the main paper.

B. Implementation Details

We evaluate our method on three widely adopted open-source VLMs: Qwen2-VL-7B [1], MiniGPT-4-13B [66], and LLaVA-v1.5-13B [28]. Unless otherwise specified, the number of malicious samples used for optimization is set to 96. The steering layer is fixed at $l=20$ for 13B models and $l=14$ for the 7B model. For inference, LLaVA-v1.5 and Qwen2-VL use a temperature of 0.2 with top- $p=0.9$, while MiniGPT-4 follows its official configuration with temperature 1.0 and top- $p=0.9$.

C. Additional Experimental Results

OOD robustness. Table E evaluates the cross-attack generalization of steering vectors extracted from Jailbreak adversarial samples with $\epsilon = \frac{16}{255}$. NullSteer achieves consistently lower ASR across structured-, perturbation-, and text-only attacks on all three models. On MiniGPT-4, it attains

Table E. Transferability performance under OOD conditions. Steering vectors are obtained from Jailbreak adversarial samples generated with $\epsilon = \frac{16}{255}$, using the same α value determined on the Jailbreak validation split. Their generalization is assessed across unseen attack types, including structure-based attacks from MM-SafetyBench [31], perturbation-based variants of PGD, and text-only attacks. The ASR is computed using the HarmBench [36] classifier.

Methods		Structured-based Attack			Perturbation-based Attack						Text-only Attack
		SD	SD.TYPO	TYPO	PGD [34]		Auto-PGD [7]		MI-FGSM [11]		GCG [72]
					$\epsilon = \frac{16}{255}$	$\epsilon = \frac{32}{255}$	$\epsilon = \frac{16}{255}$	$\epsilon = \frac{32}{255}$	$\epsilon = \frac{16}{255}$	$\epsilon = \frac{32}{255}$	
MiniGPT-4	w/o defense	13.75	43.25	43.75	70.91	78.18	74.55	76.36	78.18	79.09	58.18
	ASTRA	3.75	8.75	11.25	5.45	12.73	5.45	10.91	16.37	13.64	9.09
	NullSteer	2.35	6.28	11.57	3.28	9.43	4.65	9.42	14.21	12.71	8.24
Qwen2-VL	w/o defense	20.00	61.25	38.75	74.55	80.00	76.37	77.57	80.00	78.18	81.82
	ASTRA	11.25	40.00	33.75	21.82	14.55	15.76	15.76	18.18	18.18	30.91
	NullSteer	9.86	38.50	32.53	19.95	13.86	14.28	14.35	16.83	17.28	28.58
LLaVA-v1.5	w/o defense	18.75	55.00	22.50	69.09	74.55	80.60	90.30	87.28	89.09	92.73
	ASTRA	8.75	25.00	6.25	1.82	1.82	1.21	0.61	0.00	0.00	14.55
	NullSteer	7.65	24.00	5.80	1.74	1.70	1.00	0.61	0.00	0.00	13.50

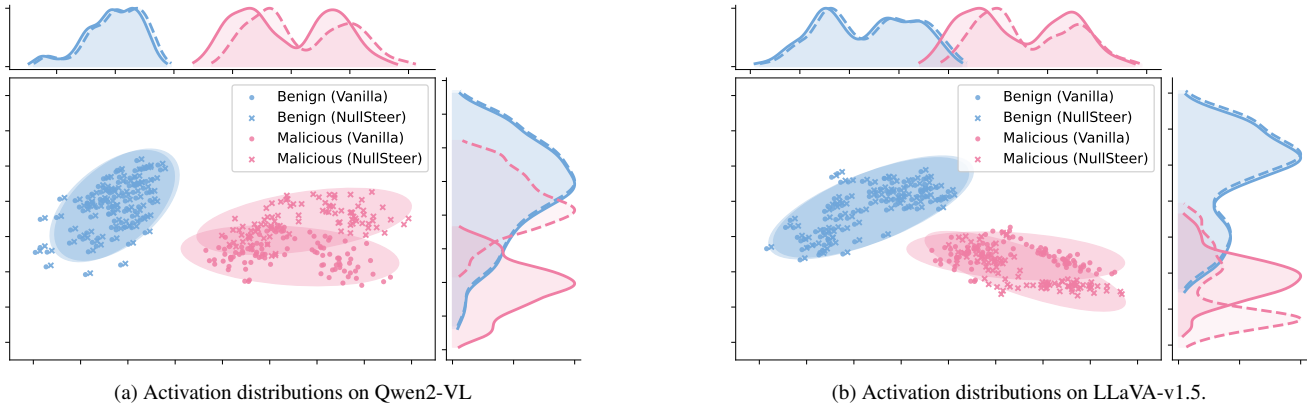


Figure I. Comparison of benign and malicious activation distributions across two VLMs.

2.35% on the SD set and 9.09% under GCG, outperforming ASTRA (3.75% and 8.24%) and the undefended model (13.75% and 58.18%). Similar patterns are observed on Qwen2-VL and LLaVA-v1.5, where NullSteer notably reduces attack success under both structured and perturbation-based attacks. These results suggest that the learned steering directions capture transferable semantics of harmful behaviors rather than attack-specific perturbations.

Activation distribution analysis. Figure I presents the activation distributions of benign and malicious inputs on Qwen2-VL and LLaVA-1.5 before and after applying NullSteer. Across both models, the benign activations under NullSteer closely overlap with their vanilla counterparts, forming compact clusters with nearly unchanged geometry. This demonstrates that the null-space constraint successfully restricts the modification to directions orthogonal to benign semantics, thereby maintaining utility. In contrast, the malicious activations exhibit a pronounced shift

away from the benign region after steering, with their density moving consistently toward safer activation directions. The clear separation between the two distributions indicates that NullSteer effectively isolates unsafe features while preserving the structure of benign representations, leading to stronger safety without sacrificing model behavior on harmless inputs.